ISSN 1070-3284, Russian Journal of Coordination Chemistry, 2023, Vol. 49, No. 9, pp. 601–611. © Pleiades Publishing, Ltd., 2023.
Russian Text © The Author(s), 2023, published in Koordinatsionnaya Khimiya, 2023, Vol. 49, No. 9, pp. 590–600.

# Specific Features of Binding Bioactive Organic Molecules with the Metallic Matrix of Heteronuclear 3*d*-4*f* Structures Containing Soft and Hard Metallocenters Using the Nd(III)–Cu(II) Complex as an Example

**M. A. Katkova[a, *], G. Yu. Zhigulin[a], E. V. Baranov[a], G. S. Zabrodina[a], M. S. Muravyeva[a, b], S. Yu. Ketkov[a], I. G. Fomina[c], and I. L. Eremenko[c]**

[a] *Razuvaev Institute of Organometallic Chemistry, Russian Academy of Sciences, Nizhny Novgorod, Russia*

[b] *Privolzhsky Research Medical University, Nizhny Novgorod, Russia*

[c] *Kurnakov Institute of General and Inorganic Chemistry, Russian Academy of Sciences, Moscow, Russia*

**e-mail: marina@iomc.ras.ru*

Received February 21, 2023; revised March 21, 2023; accepted March 22, 2023

**Abstract**—The polynuclear alanine hydroximate metallamacrocyclic complex $Nd(C_8H_7NO_4)(H_2O)[15\text{-}MC_{Cu(II)Alaha}\text{-}5](CH_3COO)$ with the axial 3-hydroxy-4-pyridinone ligand is synthesized for the first time from the (3-hydroxy-2-methyl-4-oxo-4*H*-pyridin-1-yl) acetate ligand. The X-ray diffraction (XRD) (CIF file CCDC no. 2242224) and quantum chemical methods show that the interaction of ligand L with the $Nd^{3+}$ ion retained due to ionic bonds with the oxygen atoms in the copper-containing metallamacrocyclic matrix results in the formation of axial bonds (having a covalent contribution) between $Nd^{3+}$ and the dioxolene fragment of the pyridinone ligand. In topological and energy characteristics, these axial bond approach the bonds of $Cu^{2+}$ with the amine nitrogen atoms of the alanine hydroximate metallamacrocycle.

**Keywords:** polynuclear metallamacrocyclic complexes, neodymium(III), copper(II), 3-hydroxy-4-pyridinone, molecular structure, XRD, DFT calculations

**DOI:** 10.1134/S107032842360047X

## INTRODUCTION

The polynuclear metallamacrocyclic complexes based on the biologically active α-aminohydroxymate ligands represent a unique class of heteronuclear metallacrowns (MC) that structurally resemble crown ethers [1–5]. The water-soluble Ln(III)–Cu(II) aqua complexes of MC have previously been synthesized using our original synthetic approach [6, 7] and characterized by XRD. A specific feature of the structures of the lanthanide(III)–copper(II) complexes is the planar or nearly planar metallamacrocycle consisting of five Cu(II) ions, five aminohydroximate ligands, central $Ln^{3+}$ ion coordinately bound to five oxime oxygen atoms of the metallacycle, and apical water molecules (Scheme 1) [6–10]. This structure provides a potential possibility for the axial coordination of additional anionic ligands with the lanthanide atom.

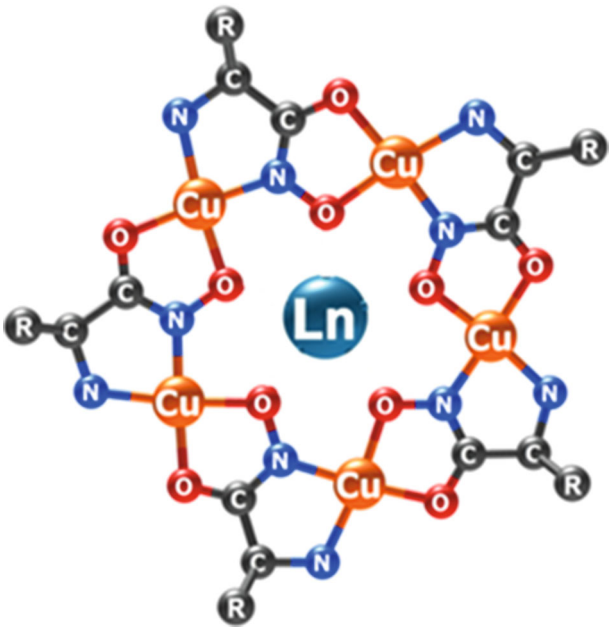


**Scheme 1.**

Organic carboxylates are among the axial ligands of the MC complexes studied in most detail since 2001 [11]. Their study showed a possibility of the application of the Ln(III)–Cu(II) MC complexes for molecular recognition and sensorics of biologically significant objects [12–18]. Chelate ligands containing along with carboxylate groups additional functional groups capable of coordinating to the metal are of evident interest from the viewpoint of the chemistry of lanthanide coordination compounds. For instance, the introduction of the hydroxy group into the α-position to the carboxy group leads to the formation of the energetically favorable planar chelate five-membered cycle Ln–O–C–C–O. This favored a successful accomplishment of the recognition of optical isomers of α-hydroxy acids in the presence of the Ln(III)–Cu(II) MC complexes [19, 20].

The chelate bioactive ligands bearing 3-hydroxy-4-pyridinone fragments together with carboxylate groups are of doubtless interest (Scheme 2). The 3-hydroxy-4-pyridinone derivatives are well known due to their biomedical applications [21, 22]. They are components of many biologically active substances of natural origin and synthetic drugs [23, 24]. However, no MC complexes with 3-hydroxy-4-pyridinone ligands have not been studied yet.

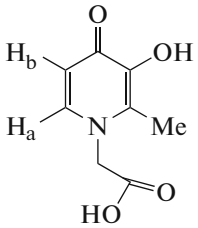


**Scheme 2.**

The purpose of this work is to synthesize new polynuclear alanine hydroximate metallamacrocyclic Nd(III)–Cu(II) complex with the axial (3-hydroxy-2-methyl-4-oxo-4*H*-pyridin-1-yl) acetate ligand (L) in order to establish a possibility of binding biologically active ligands of the pyridinone type by the alanine hydroximate metallacrowns.

## EXPERIMENTAL

Water-soluble aqua-Nd(III) polynuclear metallacyclic alanine hydroximate complex $Nd(H_2O)_4[15\text{-}MC_{Cu(II)Alaha}\text{-}5](Cl)_3$ synthesized earlier according to the developed procedures [7, 8] and (3-hydroxy-2-methyl-4-oxo-4*H*-pyridin-1-yl)acetic acid synthesized using a described procedure [25] were used as the objects of the study.

Elemental analysis was carried out on a EuroVector CHNS-O Elemental Analyzer Euro EA 3000 elemental analyzer. IR spectra were recorded on a Perkin Elmer Spectrum 65LS FT-IR spectrometer (400–4000 cm$^{-1}$) using the attenuated total internal reflectance (ATR) method. The electronic absorption spectra of the complexes were detected on an SF-56 spectrophotometer at room temperature. NMR spectra were recorded on a Bruker Avance III spectrometer (400 MHz). The samples were dissolved in a 90% $H_2O$–10% $D_2O$ mixture. 1D $^1$H NMR spectra were detected at room temperature (23°C) using the Noesygppr1d pulse sequence (Bruker) in which the signal presaturation method was used for water signal decoupling. The spectra were processed using the Bruker TopSpin 3.5 pl7 program.

**Synthesis of complex $Nd(C_8H_7NO_4)(H_2O)[15\text{-}MC_{Cu(II)Alaha}\text{-}5](CH_3COO)\cdot nH_2O$ (I).** A solution of $Ca(CH_3COO)_2H_2O$ (0.176 g, 1 mmol) in water (20 mL) was added to a hot aqueous solution of (3-hydroxy-2-methyl-4-oxo-4*H*-pyridin-1-yl)acetic acid (0.366 g, 2 mmol). The reaction mixture was refluxed using an air condenser for 1 h. A solution of alanine hydroximate metallacrown $Nd(H_2O)_4[15\text{-}MC_{Cu(II)Alaha}\text{-}5](Cl)_3$ (1.31 g, 1 mmol) was added to the obtained orange solution. The reaction mixture was stirred at 80°C for 6 h. The formed dark blue solution was filtered and stored at room temperature. The formed crystals suitable for XRD were decanted from the mother liquor and dried in air. The yield of blue crystals of compound **I** was 0.48 g (33%).

| For $C_{25}H_{67}N_{11}O_{29.5}Cu_5Nd$ | | | |
|---|---|---|---|
| Anal. calcd., % | C, 20.63 | H, 4.64 | N, 10.58 |
| Found, % | C, 20.58 | H, 4.70 | N, 10.55 |

IR (ν, cm$^{-1}$): 3236, 3142, 2984, 2936, 1657, 1648, 1576, 1542, 1446, 1398, 1372, 1290, 1169, 1100, 1063, 980, 914, 884, 806, 722, 645, 620, 587, 554, 477. $^1$H NMR (90% $H_2O$–10% $D_2O$; 400 MHz), δ: 8.34 (br.s, 1H, $H_b$), 7.89 (s, 1H, $H_a$), 2.95 (s, 3H, $CH_3$), 2.80 (s, 3H, $CH_3$).

**XRD** of a single crystal of complex **I** was conducted on an Agilent Xcalibur E automated four-circle diffractometer (Mo$K_\alpha$ radiation, ω scan mode, λ = 0.71073 Å). Diffraction data were collected, initial indexing of reflections was performed, unit cell parameters were refined, and an experimental set of intensities was integrated using the CrysAlisPro program [26]. An absorption correction was applied empirically using the SCALE3 ABSPACK algorithm [27]. The structure was solved by direct methods via the dual-space algorithm in the SHELXT program [28]. Non-hydrogen atoms were refined by full-matrix least squares for $F^2_{hkl}$ in the anisotropic approximation using the SHELXTL program package [29, 30]. Hydrogen atoms were placed in geometrically calculated positions and refined isotropically by the riding model with fixed thermal parameters ($U_{iso}$(H) = 1.5$U_{eq}$(C) for $CH_3$ groups, $U_{iso}$(H) = 1.2$U_{eq}$(C) for other groups). The H atoms of the water molecules were localized from the difference Fourier electron density synthesis are refined in the isotropic approxi-

**Table 1.** Crystallographic data and experimental structure refinement parameters for compound **I**

| Parameter | Value |
|---|---|
| Empirical formula | $C_{25}H_{67}N_{11}O_{29.50}Cu_5Nd$ |
| *FW* | 1455.83 |
| Temperature, K | 100(2) |
| Crystal system | Orthorhombic |
| Space group | $P2_12_12_1$ |
| *a*, Å | 16.5132(2) |
| *b*, Å | 16.9849(2) |
| *c*, Å | 17.6708(2) |
| *V*, Å$^3$ | 4956.22(10) |
| *Z* | 4 |
| $\rho_{calc}$, g/cm$^3$ | 1.951 |
| μ, mm$^{-1}$ | 3.237 |
| Crystal size, mm | 0.449 × 0.211 × 0.164 |
| *F*(000) | 2940 |
| Range of data collection over 2θ, deg | 2.07–30.51 |
| Number of measured / independent reflections | 104 136/15 134 |
| $R_{int}$ | 0.0934 |
| $R_1$, $wR_2$ ($I > 2\sigma(I)$) | 0.0395, 0.0840 |
| $R_1$, $wR_2$ (for all data) | 0.0507, 0.0889 |
| *S* | 1.064 |
| Absolute structure parameter | –0.029(6) |
| Residual electron density (max/min), e/Å$^3$ | 2.283/–2.096 |

mation. Solvate water molecules in a ratio of 8.5 : 1 to the molecule of the cationic neodymium complex were revealed in the crystal of complex **I**. The graphical images of the molecular and crystal structures of complex **I** were drafted in the OLEX2 program [31]. The main crystallographic characteristics and XRD experimental parameters for compound **I** are given in Table 1. Selected bond lengths and bond angles are listed in Table 2.

The structure of compound **I** was deposited with the Cambridge Crystallographic Data Centre (CIF file CCDC no. 2242224; available at ccdc.cam.ac.uk/getstructures).

**Quantum chemical calculation procedure.** The full DFT geometry optimization of complex $\{Nd(L)(H_2O)[15\text{-}MC_{Cu(II)Alaha}\text{-}5]\}^+$ was performed using the Priroda 20 program package [32, 33]. The Priroda software was shown to be capable of correct modeling complicated polynuclear complexes of 3*d* and 4*f* elements [34–36]. The PBE functional [37] combined in the four-component one-electron scalar relativistic (SR) approximation of the full Dirac equation (in which the spin-orbital terms are neglected) was used in the calculations. The triple split valence all-electron relativistic correlation consistent L2 basis set (analog of cc-pVTZ) from the b4s.in family was applied for all atoms [38]. The DFT simulation of 15-metallacrowns-5 of rare-earth elements in the high-spin state is well consistent with the experimental results [39, 40]. Therefore, the $\{Nd(L)(H_2O)[15\text{-}MC_{Cu(II)Alaha}\text{-}5]\}^+$ complex was modeled as a high-spin system with the maximum multiplicity ($M = 9$, nonet). The gradient at which the geometry optimization in Priroda 20 is finished is $10^{-5}$. The specified accuracy of the solution of the self-consistent field (SCF) equation is $10^{-8}$ at an accuracy of the numerical integration network of $10^{-9}$. The SCF equations were solved via the Newton–Raphson algorithm with allowance for small density

**Table 2.** Selected bond lengths (*d*) for complex **I**

| Bond | *d*, Å |
|---|---|
| Nd(1)–O(oxime) | 2.436(4)–2.527(4) |
| Nd(1)–O(aq) | 2.503(4) |
| Nd(1)–O(L) | 2.356(4), 2.444(4) |
| Cu–O (15-MC-5) | 1.929(4)–1.961(4) |
| Cu–N (15-MC-5) | 1.900(5)–2.034(5) |
| Cu–O(aq) | 2.373(5)–2.621(5) |

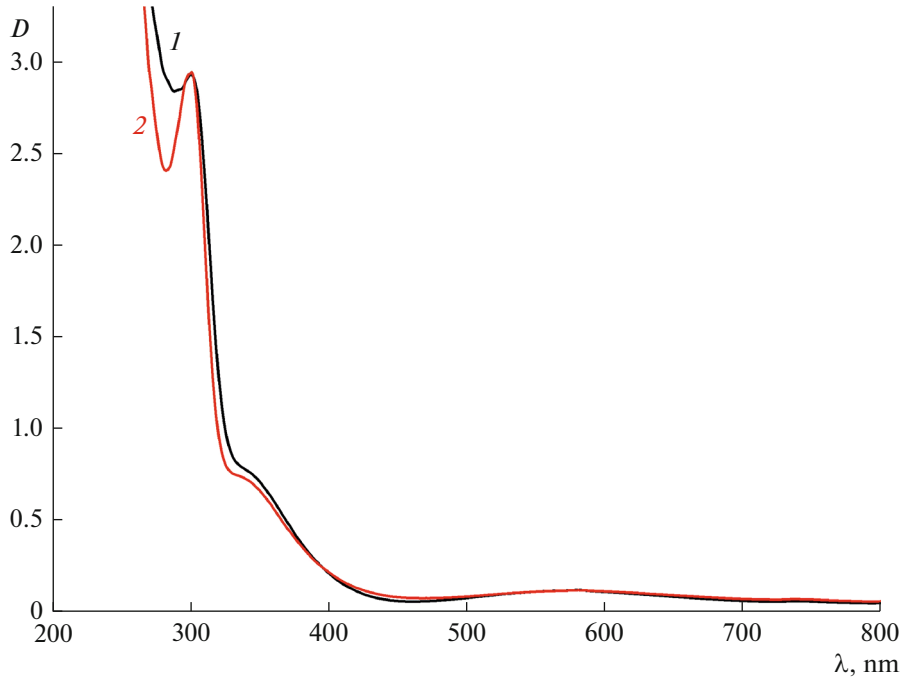


**Fig. 1.** Electronic absorption spectra of complex **I** ($c = 0.4$ mM) in (*1*) a physiological solution (pH 7.0) and (*2*) an isotonic phosphate buffer (pH 7.4).

components (key words proc = NR and d1small = 1 in the Priroda code). For the optimized structure of $\{Nd(L)(H_2O)[15\text{-}MC_{Cu(II)Alaha}\text{-}5]\}^+$, whose electron energy is −20531.73084878 au, the electron densities $\rho(\mathbf{r}_c)$ at the critical points, and $\lambda_1$, $\lambda_2$, and $\lambda_3$ eigenvalues of the Hessian $A(\mathbf{r}_c)$ were obtained in Priroda 20. The values of the density Laplacian $\nabla^2\rho(\mathbf{r}_c)$ were calculated by Eq. (1) [41]. The densities of the kinetic electronic energy $G(\mathbf{r}_c)$ were calculated from Abramov's approximation (2) [42]. The densities of the potential electronic energy $V(\mathbf{r}_c)$ were calculated according to the virial theorem (3) [41]. The energies of interatomic distances $E$ were calculated by the Espinosa equation (4) [43].

$$\nabla^2\rho(\mathbf{r}_c) = \lambda_1 + \lambda_2 + \lambda_3, \quad (1)$$

$$G(\mathbf{r}_c) = (3/10)(3\pi^2)^{2/3}\rho(\mathbf{r}_c)^{5/3} + (1/6)\nabla^2\rho(\mathbf{r}_c), \quad (2)$$

$$V(\mathbf{r}_c) = (1/4)\nabla^2\rho(\mathbf{r}_c) - 2G(\mathbf{r}_c), \quad (3)$$

$$E = -(1/2)V(\mathbf{r}_c). \quad (4)$$

The spin density isosurfaces, electron localization functions $\eta(\mathbf{r})$ (ELF) [44, 45], and reduced density gradients $s(\mathbf{r})$ (RDG) [46] were obtained in Gabedit 2.5.0 [47] from the wave function of the structure optimized in Priroda 20. The set of $\eta(\mathbf{r})$ specified for the construction of the ELF maps is described by dependence (5) in which $N$ is the natural number from 1 to 9 inclusive. The RDG isosurface was obtained according to Eq. (6) at $\rho(\mathbf{r}) \le 0.05$ au.

$$\eta(\mathbf{r}) = -N^2/200 + (19/200)N + 9/20, \quad (5)$$

$$s(\mathbf{r}) = |\nabla\rho(\mathbf{r})|/(2(3\pi^2)^{1/3}\rho(\mathbf{r})^{4/3}). \quad (6)$$

## RESULTS AND DISCUSSION

We synthesized complex $Nd(C_8H_7NO_4)(H_2O)[15\text{-}MC_{Cu(II)Alaha}\text{-}5](CH_3COO)\cdot nH_2O$ (**I**) continuing the studies of the influence of the Ln(III)–Cu(II) structure of the alanine hydroximate metallacrown and nature of the pyridinone type ligand on the formation of new polyfunctional compounds. The reaction products were isolated as single crystals and characterized by CHN analysis, IR spectroscopy, and XRD. The stability of the synthesized complex was studied in a physiological solution (pH 7.0) and an isotonic phosphate buffer (pH 7.4) (Fig. 1). Complex **I** was found to be stable under these conditions for more than 2 weeks.

The $^1$H NMR spectra of the complex were compared with the spectra of the free ligand (Fig. 2). The most informative are signals from the $H_a$ and $H_b$ protons of the pyridine ring because of a higher sensitivity to the complex formation of the paramagnetic MC. For instance, a significant signal broadening and a down-field shift were observed for the $H_b$ proton (see Scheme 2 for proton numeration), the change in the $H_b$ chemical shift was 1.35 ppm (540 Hz), and that of the $H_a$ shift was 0.01 ppm (6 Hz).

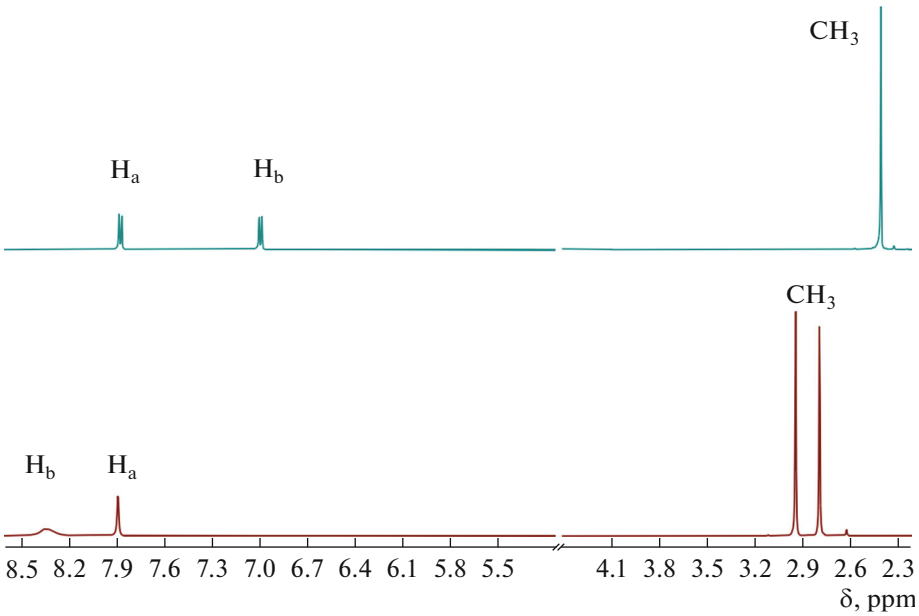


**Fig. 2.** Comparison of the $^1$H NMR spectra of the starting ligand (upper) and complex **I** (bottom).

The molecular and crystal structures of complex **I** were finally determined by XRD. Compound **I** is an ionic complex consisting of the separated cation $Nd(C_8H_7NO_4)(H_2O)[15\text{-}MC_{Cu(II)Alaha}\text{-}5]^+$ and acetate anion (Fig. 3). The Nd(1) neodymium atom is located at the center of the copper metallacrown and bound to five oxygen atoms O(1,3,5,7,9) in the equatorial plane. The Nd(1) atom is additionally coordinated by the water molecule and pyridinone ligand arranged at the apical positions. Dianionic ligand L coordinates on the lanthanide atom via the bidentate mode by the O(12) and O(13) atoms (Fig. 3b). The O(12)–C(16) and O(13)–C(17) bond lengths are 1.305(7) and 1.330(7) Å, respectively, and coincide with similar distances in the $La(Dpp)_3$ complex containing related 3-hydroxy-1,2-dimethylpyridin-4-one ligands (Dpp) (1.285(3)–1.330(3) Å) [48]. The metal–ligand distances Nd(1)–O(12) and Nd(1)–O(13) are noticeably differentiated being 2.444(4) and 2.356(4) Å. The C–O (C(23)–O(14) and C(23)–O(15)) distances in the pyridinone ligand are equalized 1.238(8) and 1.253(8) Å) indicating the carboxylate character of the C(23)O(14)O(15) fragment similarly to the initial 3-hydroxy-1-carboxymethyl-2-methyl-4-pyridinone compound (1.226(2)– 1.273(2) Å [25, 49]). Note that the C–O bond lengths differ appreciably (1.233(9), 1.268(9), and 1.20(1), 1.35(1) Å, respectively) in the structure related to the pyridine ligand, 1-(3-hydroxymethyl-2-methyl-4-oxopyridyl)-1,3-propane-dicarboxylic acid [50] bearing two functional groups: carboxylate (ionic) and carboxyl (neutral). The acetate anion is an outer-sphere molecule and arranged above the plane of the copper metallamacrocycle near the water molecule coordinated to Nd(1). The C(24)–O(20) and C(24)–O(21) bond lengths in the acetate anion are 1.271(9) and 1.262(8) Å and close to similar distances in the carboxylate group of the pyridine substituent.

The copper metallamacrocycle 15-MC-5 is nonplanar and has a slightly wavy shape. The average deviation of the non-hydrogen atoms of the metallacycle fragment from the plane is 0.32 Å. The Nd(1) neodymium atom is shifted from the metallacrown plane by 0.024(1) Å toward the pyridinone ligand. The sum of the ONd(1)O angles between the substituents in the equatorial plane is 354.4°. The angles between the apical substituents are 150.54(14)° and 142.74(14)°. The chelate angle of the pyridinone ligand is 66.40(14)°.

The Cu(1) and Cu(3–5) copper atoms in the metallacrown are additionally coordinated by the water molecules and, thus, have a square pyramidal environment. Two pairs of water molecules with the oxygen atoms O(16), O(18) and O(17), O(19), respectively, are arranged at different sides from the metallacrown plane. The water molecules with the O(16) and O(18) atoms, along with the coordination on the Cu(1) and Cu(4) atoms, additionally interact with the pyridinone ligand via the hydrogen bonds O(16)–H...O(13) (1.81(3) Å) and O(18)–H...O(12) (1.74(3) Å). The pair of water molecules (O(11) and O(19)) coordinated to Nd(1) and Cu(5), respectively, bind the outer-sphere acetate anion due to the hydrogen bonds O(11)–H...O(21) (1.84(3) Å) and O(19)–H...O(21) (1.87(2) Å).

Note that four of five methyl substituents of alanine hydroximates are arranged above the metallacrown plane. The shift of the Me groups from this plane varies in a range of 1.690(6)–2.178(8) Å toward the pyridinone ligand. The fifth methyl group lies almost in the

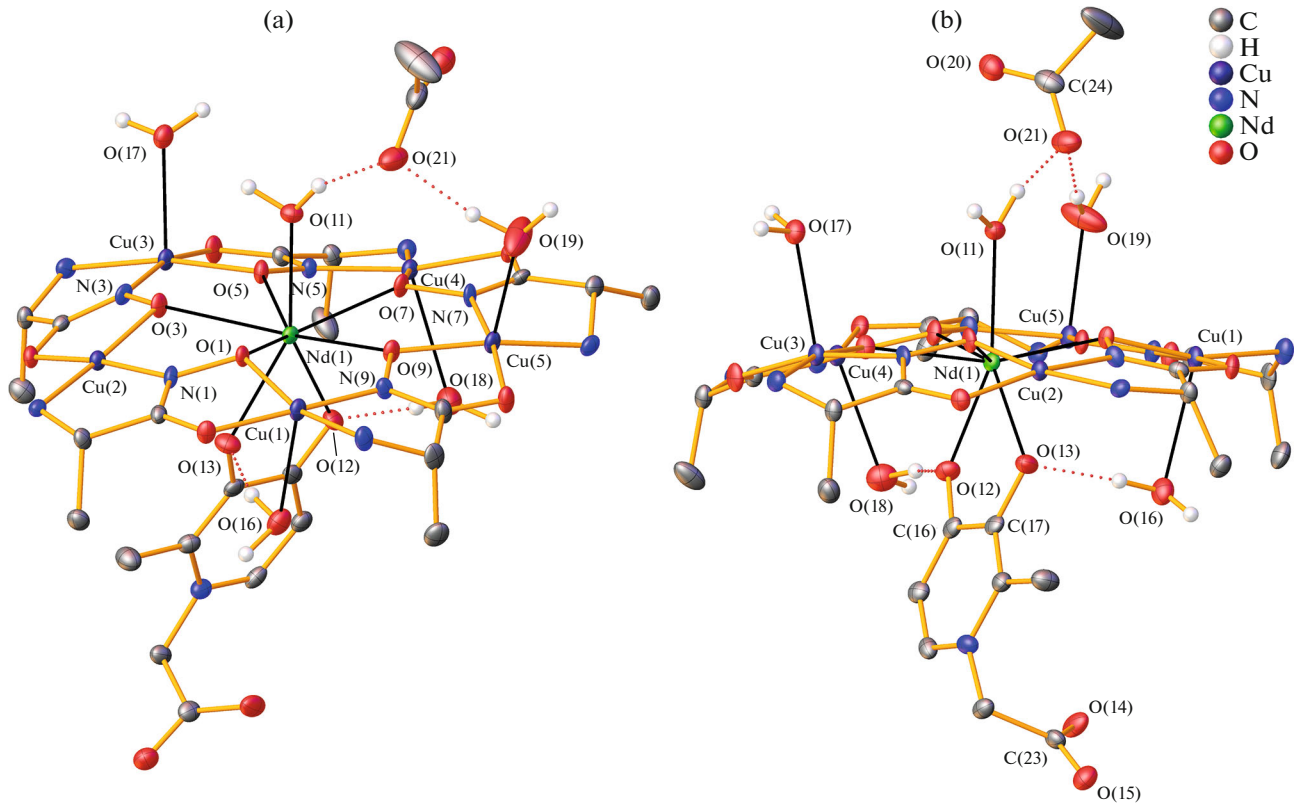


**Fig. 3.** (a) General and (b) profile view of the molecular structure of complex **I**. Thermal ellipsoids of atoms are given with 50% probability. The solvate molecules and hydrogen atoms, except for the H atoms of coordinated $H_2O$ molecules, are omitted.

metallacrown plane, and its shift from the plane is 0.343(7) Å also insignificantly shifting toward pyridinone.

One-dimensional chains of the neodymium complex molecules are formed by the intermolecular contacts Cu(2)...O(8) (2.671(4) Å) along the crystallographic axis *b* in the crystal of compound **I** (Fig. 4a). The molecules of the Nd(III) complex in the chains are arranged in the syndiotactic order. The coordination number of the Cu(2) atom is 5, and the coordination sphere of Cu(2) is characterized by a square pyramidal configuration. The 1D chains form along the *c*0*b* plane packing layers of two types alternating along the *a* axis of the crystal (Fig. 4b).

The quantum chemical modeling of the steric and electronic structures was performed for the cationic form of the complex $\{Nd(L)(H_2O)[15\text{-}MC_{Cu(II)Alaha}\text{-}5]\}^+$. The corresponding calculations were performed at the SR-PBE/L2 level of the density functional theory (DFT). The geometry optimization for $\{Nd(L)(H_2O)[15\text{-}MC_{Cu(II)Alaha}\text{-}5]\}^+$ results in the structure in which the carboxylate fragment of the 3-hydroxy-4-pyridinone ligand interacts with the $NH_2$ group of the alanine hydroximate ligand (Fig. 5). The deviation from the crystal structure is due to a tendency of the 3-hydroxy-4-pyridinone ligand to compensate the intrinsic negative charge. Unlike the crystalline matrix, the model of the isolated $\{Nd(L)(H_2O)[15\text{-}MC_{Cu(II)Alaha}\text{-}5]\}^+$ complex has no additional $H_2O$ molecules that could interact with the 3-hydroxy-4-pyridinone ligand. For this cause, the O(14)···HN(10) hydrogen bond with a length of 1.628 Å appears in the DFT-optimized structure. The $H_2O(11)$ axial molecule is also characterized by an intermolecular interaction with the metallamacrocycle. The O(1)···HO(11) hydrogen bond (1.946 Å, Fig. 6) is observed in the DFT-optimized structure in the absence of an outer-sphere acetate anion. This results in a substantial reestimation of the Nd(1)–O(1) and Nd(1)–O(11) bonds (2.645 and 2.663 Å, respectively; Table 3) compared to the experiment. Other Nd–O interatomic distances, as well as Cu–O and Cu–N (exemplified by the bonds of the Cu(3) coordination node), are well consistent with the XRD data. As in the crystalline phase, the axial bonds with the 3-hydroxy-4-pyridinone ligand Nd(1)–O(12) and Nd(1)–O(13) (2.371 and 2.299 Å, respectively) are much shorter than the equatorial interactions of $Nd^{3+}$ with the oxime O atoms of the metallamacrocycle (2.469–2.584 Å without Nd(1)–O(1)). For the equatorial bonds of $Cu^{2+}$, the DFT calculations also reproduce XRD tendencies. In particular, the Cu(3)–N(4)

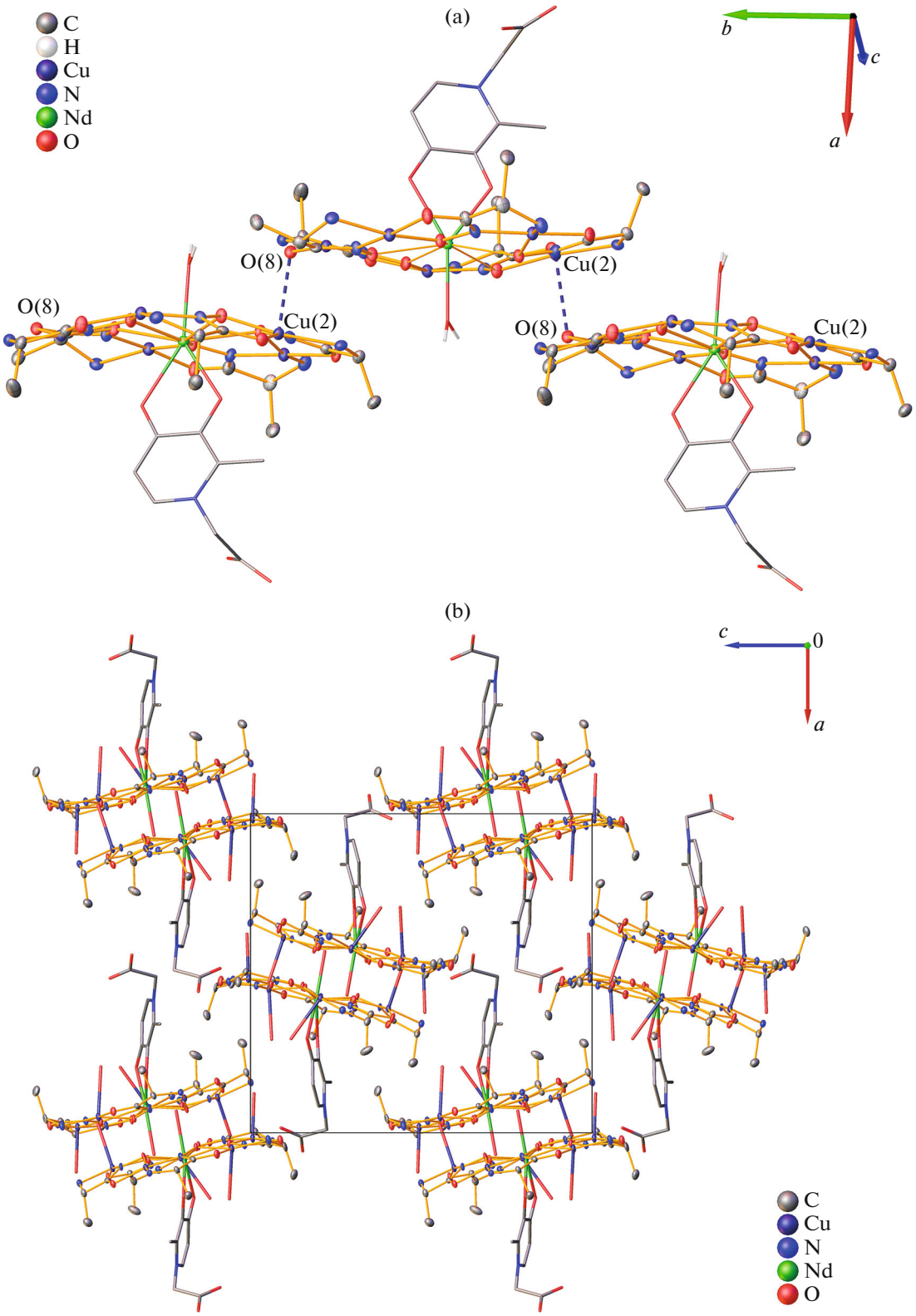


**Fig. 4.** Fragments of (a) the 1D chain and (b) packing of complex **I** in the crystal. The hydrogen atoms, acetate anion, and some water molecules are omitted.

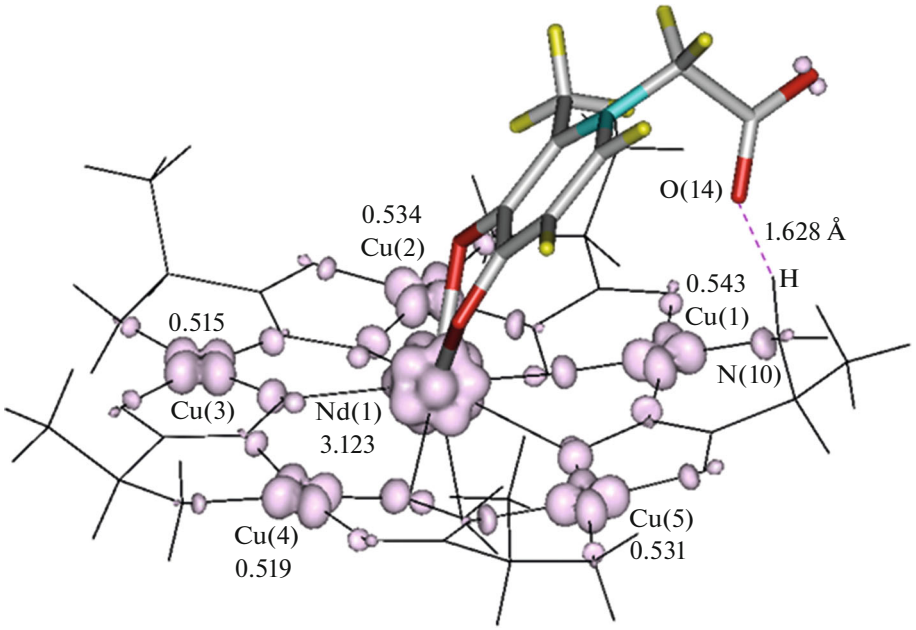


**Fig. 5.** Spin density distribution (isosurface at 0.03 au) for the optimized structure of the $\{Nd(L)(H_2O)[15\text{-}MC_{Cu(II)Alaha}\text{-}5]\}^{+}$ complex with the indication of Mulliken spin populations.

distance is maximum (2.075 Å) and Cu(3)–N(3) is minimum (1.905 Å).

The Mulliken spin densities for the $Cu^{2+}$ ions lie in a range of 0.515–0.543, which reveals the spin density delocalization in the coordination environment of $Cu^{2+}$ (Fig. 5). On the one hand, the spin density distribution directly around the Cu nucleus corresponds to the topology of the 3*d* orbital. On the other hand, the spin population for $Nd^{3+}$ is 3.123 indicating the total localization of three lone 4*f* electrons in the vicinity of the Nd nucleus. The spin density distribution corresponds to the local symmetry $I_h$. In other words, the spin density isosurface around the Nd nucleus can be inscribed into an icosahedron. In Fig. 5, the structure of the complex is oriented in such a way that an observer can see 11 of 12 domains of the isosurface around the Nd nucleus corresponding to the isocahedron vertices. Six pronounced domains in front correspond to the vertices of one of two pentagonal pyra-

**Table 3.** Topological parameters (au) of the $\{Nd(L)(H_2O)[15\text{-}MC_{Cu(II)Alaha}\text{-}5]\}^{+}$ complex at the critical points (3,−1) and energies of interatomic interactions (kcal/mol)

| Bond | *d*, Å (DFT) | $\rho(\mathbf{r}_c)$ | $\nabla^2\rho(\mathbf{r}_c)$ | $V(\mathbf{r}_c)$ | $G(\mathbf{r}_c)$ | $\lvert V(\mathbf{r}_c)\rvert/G(\mathbf{r}_c)$ | *E* |
|---|---|---|---|---|---|---|---|
| Nd(1)–O(1) | 2.645 | 0.0313 | 0.126 | −0.0284 | 0.0300 | 0.95 | 8.9 |
| Nd(1)–O(3) | 2.543 | 0.0397 | 0.157 | −0.0396 | 0.0394 | 1.00 | 12.4 |
| Nd(1)–O(5) | 2.469 | 0.0465 | 0.188 | −0.0502 | 0.0487 | 1.03 | 15.8 |
| Nd(1)–O(7) | 2.584 | 0.0368 | 0.141 | −0.0351 | 0.0351 | 1.00 | 11.0 |
| Nd(1)–O(9) | 2.535 | 0.0408 | 0.160 | −0.0411 | 0.0405 | 1.01 | 12.9 |
| Nd(1)–O(11) | 2.663 | 0.0318 | 0.121 | −0.0283 | 0.0292 | 0.97 | 8.9 |
| Nd(1)–O(12) | 2.371 | 0.0620 | 0.231 | −0.0750 | 0.0663 | 1.13 | 23.5 |
| Nd(1)–O(13) | 2.299 | 0.0731 | 0.263 | −0.0953 | 0.0806 | 1.18 | 29.9 |
| Cu(3)–N(3) | 1.905 | 0.1114 | 0.474 | −0.1876 | 0.1531 | 1.23 | 58.9 |
| Cu(3)–N(4) | 2.075 | 0.0765 | 0.314 | −0.1053 | 0.0919 | 1.15 | 33.0 |
| Cu(3)–O(5) | 1.952 | 0.0887 | 0.486 | −0.1417 | 0.1316 | 1.08 | 44.5 |
| Cu(3)–O(6) | 1.953 | 0.0881 | 0.487 | −0.1407 | 0.1312 | 1.07 | 44.1 |
| O(14)···HN(10) | 1.628 | 0.0559 | 0.121 | −0.0569 | 0.0436 | 1.31 | 17.9 |
| O(1)···HO(11) | 1.946 | 0.0290 | 0.059 | −0.0207 | 0.0178 | 1.16 | 6.5 |

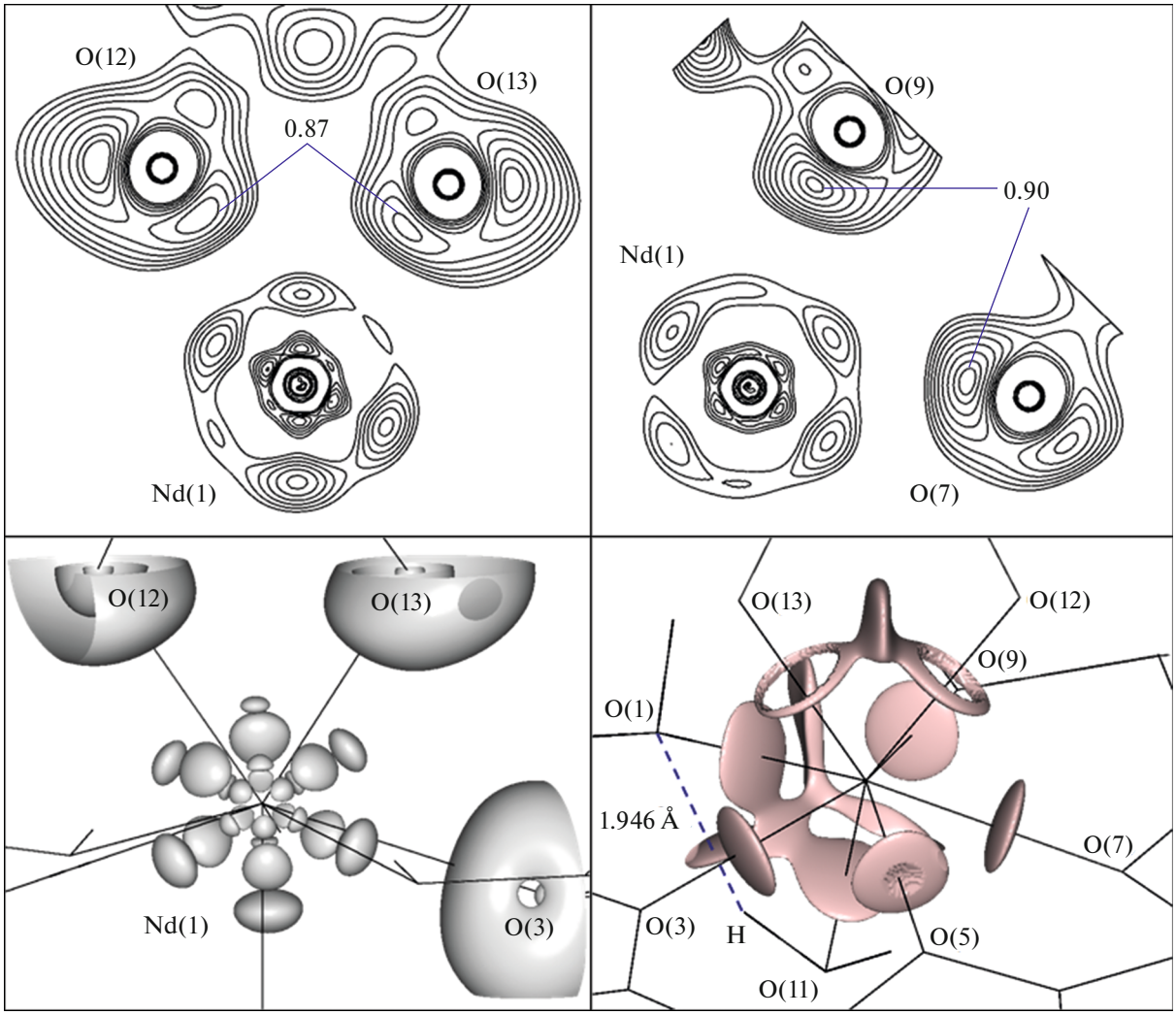


**Fig. 6.** Electronic structure of the $\{Nd(L)(H_2O)[15\text{-}MC_{Cu(II)Alaha}\text{-}5]\}^+$ complex. Maps of the ELF distribution in the planes of the atoms O(12), O(13), and Nd(1) (at upper left) and O(9), O(7), and Nd(1) (at upper right); ELF contours: 0.54, 0.62, 0.69, 0.75, 0.80, 0.84, 0.87, 0.89, and 0.90. Isosurfaces of ELF at $\eta(\mathbf{r}) = 0.76$ (at bottom left) and RDG at $s(\mathbf{r}) = 0.5$ (at bottom right) in the vicinity of the Nd(1) nucleus.

mids forming an isosahedron. The $I_h$ symmetry of the spin density isosurface around the Nd nucleus is a result of the superposition of the 4*f* orbitals of three lone electrons of the $Nd^{3+}$ ion.

A topological analysis of the electron density of the $\{Nd(L)(H_2O)[15\text{-}MC_{Cu(II)Alaha}\text{-}5]\}^+$ complex was performed in terms of the quantum theory of atoms in molecules (QTAIM) [41]. Low electron densities $\rho(\mathbf{r}_c)$ and positive Laplacians $\nabla^2\rho(\mathbf{r}_c)$ are observed at the critical points (3,−1) of the Nd–O, Cu–O, and Cu–N bonds, as well as the O(14)···HN(10) and O(1)···HO(11) contacts, which is a property of polar interactions (Table 3). The QTAIM formalism makes it possible to classify types of interatomic contacts. One of the classification criteria is the ratio of the modulus of the potential electronic energy density $V(\mathbf{r}_c)$ to the kinetic electronic energy density $G(\mathbf{r}_c)$ [51, 52]. The values $|V(\mathbf{r}_c)|/G(\mathbf{r}_c) < 1$ describe the contacts of the "closed" atomic shells, particularly, ionic bonds. The values $|V(\mathbf{r}_c)|/G(\mathbf{r}_c) > 2$ characterize the "generalized" interactions (covalent bonds). In the QTAIM terminology, the range $1 < |V(\mathbf{r}_c)|/G(\mathbf{r}_c) < 2$ corresponds to "intermediate" interactions. The calculated values $|V(\mathbf{r}_c)|/G(\mathbf{r}_c) = 0.95–1.03$ make it possible to consider the Nd–O equatorial bonds and Nd(1)–O(11) as ionic interactions. On the one hand, the $|V(\mathbf{r}_c)|/G(\mathbf{r}_c)$ ratios close to 1 for the bonds of rare-earth cations with the O oxime atoms in 15-metallacrowns-5 are also predicted by the DFT calculations with the pseudopotential basis sets [9, 53]. On the other hand, increased values $|V(\mathbf{r}_c)|/G(\mathbf{r}_c) = 1.13$ and 1.18 for Nd(1)–O(12) and Nd(1)–O(13), respectively, indicate a stronger density donation. The corresponding values $\rho(\mathbf{r}_c) = 0.0620$ and 0.0731 au and the bond

energies $E = 23.5$ and 29.9 kcal/mol for Nd(1)–O(12) and Nd(1)–O(13) are maximum compared to those for other Nd–O bonds. Interestingly, the "hard" (in energy) Nd(1)–O(12) and Nd(1)–O(13) interactions approach the "softer" Cu(3)–N(4) bond (33.0 kcal/mol), which is least strong among the equatorial bonds of Cu(3). The "intermediate" interaction of Cu(3) with the imine N(3) atom is characterized by the highest covalent contribution ($|V(\mathbf{r}_c)|/G(\mathbf{r}_c) = 1.23$) and energy ($E = 58.9$ kcal/mol) among the considered metal–ligand bonds. On the whole, the classification of the Cu(3) bonds as "intermediate" agrees with the known QTAIM studies of the Cu(II) aminohydroximate complexes based on the DFT calculations [54]. A substantial difference in estimates of the energies of the O(14)···HN(10) and O(1)···HO(11) hydrogen bonds ($E$ = 17.9 and 6.5 kcal/mol, respectively) is caused by the difference in their lengths (1.628 and 1.946 Å).

The results obtained in the QTAIM framework are consistent with the distribution of the electron localization function $\eta(\mathbf{r})$ (ELF) [44, 45]. The domains of lone electron pairs of the O(12) and O(13) atoms of the 3-hydroxy-4-pyridinone ligand interacting with $Nd^{3+}$ are characterized by the maxima $\eta(\mathbf{r}) = 0.87$ in the O(12), O(13), and Nd(1) plane (Fig. 6). In the case of the domains of lone pairs of the O(9) and O(7) oxime atoms oriented to the Nd nucleus, the electron localization is more pronounced and the maxima of the function reach $\eta(\mathbf{r}) = 0.90$. An increase in the electron localization in the vicinity of the nonmetal nucleus corresponds to a concept of a decrease in the density donating to the metal. The violation of the spherical distribution of the external and external atomic shells of Nd is caused by the influence of 4*f* electrons. Thus, the ELF topology is consistent with the commonly accepted concepts about the penetration of 4*f* electrons into the inert shells of the $Ln^{3+}$ ions [55]. As the spin density distribution in the vicinity of the Nd nucleus, the topology of the cage basin of Nd (C(Nd) in the ELF terminology) corresponds to the icosahedron symmetry (Fig. 6). In this case, the external shell of the $Nd^{3+}$ ion undergoes perturbation from the 3-hydroxy-4-pyridinone ligand (namely, O(12) and O(13) atoms), which violates the ideal symmetry $I_h$ of the external shell compared to the internal shell.

An analysis of the reduced density gradient $s(\mathbf{r})$ (RDG) makes it possible to observe a range of noncovalent interactions (NCI) [46]. At $s(\mathbf{r}) = 0.5$ (Fig. 6) in the vicinity of the Nd nucleus, six disk-like domains corresponding to the Nd–O equatorial ionic bonds and axial Nd(1)–O(11) bond are revealed. In the case of more covalent interactions Nd(1)–O(12) and Nd(1)–O(13) (instead of analogous domains), the RDG isosurface takes a residual toroidal shape. The RDG range between the atoms forming the O(1)···HO(11) hydrogen bond is also observed in Fig. 6.

Thus, the QTAIM, ELF, and RDG studies based on the DFT calculations predict a strong binding of the biologically active ligands of the pyridinone type with alanine hydroximate metallacrowns. The axial interactions of the 3-hydroxy-4-pyridinone ligand with the $Nd^{3+}$ ion exceed in energy the equatorial ionic bonds of $Nd^{3+}$ with the macrocycle. This caused the stability of the complex in the crystalline phase and also in an aqueous solution where properties of dissociation to the starting macrocycle and pyridinone ligand are absent.

## ACKNOWLEDGMENTS

XRD and NMR spectroscopy were carried out using the equipment of the Center for Collective Use at the Razuvaev Institute of Organometallic Catalysis (Russian Academy of Sciences) in the area of basic research. IR spectroscopy, and C,H,N analyses were carried out using the equipment of the Center for Collective Use of Physical Methods of Investigation at the Kurnakov Institute of General and Inorganic Chemistry (Russian Academy of Sciences) supported by the state assignment of the Kurnakov Institute of General and Inorganic Chemistry (Russian Academy of Sciences) in the area of basic research.

## FUNDING

Quantum chemical calculations were performed by G.Yu. Zhigulin and supported by the Russian Science Foundation, project no. 22-73-00285 (https://rscf.ru/project/22-73-00285/).

## CONFLICT OF INTEREST

The authors of this work declare that they have no conflicts of interest.

## REFERENCES

1. *Advances in Metallacrown Chemistry*, Zaleski, C.M., Ed., Cham: Springer, 2022.
2. Katkova, M.A., *Russ. J. Coord. Chem.*, 2018, vol. 44, p. 284. https://doi.org/10.1134/S107032841804005X
3. Ostrowska, M., Fritsky, I.O., Gumienna-Kontecka, E., et al., *Coord. Chem. Rev.*, 2016, vols. 327–328, p. 304.
4. Tegoni, M. and Remelli, M., *Coord. Chem. Rev.*, 2012, vol. 256, p. 289.
5. Mezei, G., Zaleski, C.M., and Pecoraro, V.L., *Chem. Rev.*, 2007, vol. 107, p. 4933.
6. Katkova, M.A., Zabrodina, G.S., Muravyeva, M.S., et al., *Eur. J. Inorg. Chem.*, 2015, vol. 2015, p. 5202.
7. Katkova, M.A., Zabrodina, G.S., Baranov, E.V., et al., *Appl. Organomet. Chem.*, 2018, vol. 32, p. e4389.
8. Muravyeva, M.S., Zabrodina, G.S., Samsonov, M.A., et al., *Polyhedron*, 2016, vol. 114, p. 165.
9. Katkova, M.A., Zabrodina, G.S., Rumyantcev, R.V., et al., *Eur. J. Inorg. Chem.*, 2019, vol. 2019, p. 4328.

10. Kremlev, K.V., Samsonov, M.A., Zabrodina, G.S., et al., *Polyhedron*, 2016, vol. 114, p. 96.

11. Cutland, A.D., Halfen, J.A., Kampf, J.W., et al., *J. Am. Chem. Soc.*, 2001, vol. 123, p. 6211.

12. Lim, C.S., Kampf, J.W., and Pecoraro, V.L., *Inorg. Chem.*, 2009, vol. 48, p. 5224.

13. Tegoni, M., Tropiano, M., Marchio, L., et al., *Dalton Trans.*, 2009, p. 6705.

14. Jankolovits, J., Lim, C.S., Mezei, G., et al., *Inorg. Chem.*, 2012, vol. 51, p. 4527.

15. Jankolovits, J., Van-Noord, A.D.C., Kampf, J.W., et al., *Dalton Trans.*, 2013, vol. 42, p. 9803.

16. Pavlishchuk, A.V., Kolotilov, S.V., Zeller, M., et al., *Inorg. Chem.*, 2014, vol. 53, p. 1320.

17. Katkova, M.A., Zabrodina, G.S., Muravyeva, M.S., et al., *Inorg. Chem. Commun.*, 2015, vol. 52, p. 31.

18. Pavlishchuk, A.V., Kolotilov, S.V., Zeller, M., et al., *Eur. J. Inorg. Chem.*, 2018, vol. 2018, p. 3504.

19. Lim, C.S., Jankolovits, J., Zhao, P., et al., *Inorg. Chem.*, 2011, vol. 50, p. 4832.

20. Katkova, M.A., Baranov, E.V., Zabrodina, G.S., et al., *Macroheterocycles*, 2021, vol. 14, p. 101.

21. Rangel, M., Moniz, T., Silva, A., et al., *Pharmaceuticals*, 2018, vol. 11, p. 110.

22. Santos, M.A., Marques, S.M., and Chaves, S., *Coord. Chem. Rev.*, 2012, vol. 256, p. 240.

23. Mawani, Y., Cawthray, J.F., and Chang, S., *Dalton Trans.*, 2013, vol. 42, p. 5999.

24. Lin, S., Liu, C., Zhao, X., et al., *Front. Chem.*, 2022, vol. 10, p. 869860.

25. Zhang, Z., Rettig, S.J., and Orvig, C., *Can. J. Chem.*, 1992, vol. 70, p. 763.

26. *Data Collection, Reduction and Correction Program. CrysAlisPro 1.171.41.93a - Software Package*, Rigaku OD, 2020.

27. *SCALE3 ABSPACK: Empirical Absorption Correction. CrysAlisPro 1.171. 41.93a - Software Package*, Rigaku OD, 2020.

28. Sheldrick, G.M., *Acta Crystallogr., Sect. A: Found. Adv.*, 2015, vol. 71, p. 3.

29. Sheldrick, G.M., *SHELXTL. Version 6.14. Structure Determination Software Suite*, Madison: Bruker AXS, 2003.

30. Sheldrick, G.M., *Acta Crystallogr., Sect. C: Struct. Chem.*, 2015, vol. 71, p. 3.

31. Dolomanov, O.V., Bourhis, L.J., Gildea, R.J., et al., *J. Appl. Crystallogr.*, 2009, vol. 42, p. 339.

32. Laikov, D.N., *Chem. Phys. Lett.*, 1997, vol. 281, p. 151.

33. Laikov, D.N. and Ustynyuk, Y.A., *Russ. Chem. Bull.*, 2005, vol. 54, p. 820.

34. Zabrodina, G.S., Katkova, M.A., Rumyantcev, R.V., et al., *Macroheterocycles*, 2022, vol. 15, p. 109.

35. Svitova, A.L. and Dunsch, L., *Inorg. Chem.*, 2013, vol. 52, p. 3368.

36. Katkova, M.A., Zhigulin, G.Y., Rumyantcev, R.V., et al., *Molecules*, 2020, vol. 25, p. 4379.

37. Perdew, J.P., Burke, K., and Ernzerhof, M., *Phys. Rev. Lett.*, 1996, vol. 77, p. 3865.

38. Laikov, D.N., *Theor. Chem. Acc.*, 2019, vol. 138, p. 40.

39. Zhigulin, G.Yu., Zabrodina, G.S., Katkova, M.A., et al., *Russ. Chem. Bull.*, 2018, vol. 67, p. 1173.

40. Katkova, M.A., Zabrodina, G.S., Zhigulin, G.Yu., et al., *Russ. J. Coord. Chem.*, 2019, vol. 45, p. 721.

41. Bader, R.F.W., *Atoms in Molecules*: *A Quantum Theory*, Oxford: Oxford Univ., 1990.

42. Abramov, Y.A., *Acta Crystallogr., Sect. A: Found. Crystallogr.*, 1997, vol. 53, p. 264.

43. Espinosa, E., Molins, E., and Lecomte, C., *Chem. Phys. Lett.*, 1998, vol. 285, p. 170.

44. Becke, A.D. and Edgecombe, K.E., *J. Chem. Phys.*, 1990, vol. 92, p. 5397.

45. Savin, A., Silvi, B., and Colonna, F., *Can. J. Chem.*, 1996, vol. 74, p. 1088.

46. Johnson, E.R., Keinan, S., Mori-Sánchez, P., et al., *J. Am. Chem. Soc.*, 2010, vol. 132, p. 6498.

47. Allouche, A.R., *J. Comput. Chem.*, 2011, vol. 32, p. 174.

48. Weekes, D.M., Cawthray, J.F., Rieder, M., et al., *Metallomics*, 2017, vol. 9, p. 902.

49. Orvig, C., Rettig, S.J., and Zhang, Z., *Acta Crystallogr., Sect. C: Cryst. Struct. Commun.*, 1994, vol. 50, p. 1514.

50. Molenda, J.J., Jones, M.M., Johnston, D.S., et al., *J. Med. Chem.*, 1994, vol. 37, p. 4363.

51. Espinosa, E., Alkorta, I., Elguero, J., et al., *J. Chem. Phys.*, 2002, vol. 117, p. 5529.

52. Gibbs, G.V., Cox, D.F., Crawford, T.D., et al., *J. Chem. Phys.*, 2006, vol. 124, p. 084704.

53. Zhigulin, G.Yu., Zabrodina, G.S., Katkova, M.A., et al., *Russ. Chem. Bull.*, 2019, vol. 68, p. 743.

54. Zhigulin, G.Yu., Zabrodina, G.S., Katkova, M.A., et al., *Russ. J. Coord. Chem.*, 2019, vol. 45, p. 356. https://doi.org/10.1134/S107032841905004X

55. Greenwood, N.N. and Earnshaw, A., *Chemistry of the Elements*, Oxford: Butterworth–Heinemann, 1997.

*Translated by E. Yablonskaya*